CDF note 7896

Search for Extra Dimensions in Run II Jets plus Missing E_T Sample

The CDF Collaboration
URL http://www-cdf.fnal.gov
(Dated: October 25, 2005)

We present the results of a search for new physics in the jets plus missing transverse energy data sample collected from 368 pb^{-1} of $p\bar{p}$ collisions at $\sqrt{s} = 1.96$ TeV recorded by the Collider Detector at Fermilab. We compare the number of events observed in the data with a data-driven estimate of the Standard Model backgrounds contributing to this channel. No significant excess is observed, and we interpret this null result in terms of lower limits on the effective Planck scale (M_D) for the Large Extra Dimension scenario.

Preliminary Results for Fall 2005 Conferences

Events with large missing transverse energy and one or more energetic jets are predicted in many models for physics beyond the Standard Model (SM). SUSY with R-parity conservation [1], technicolor with the technirhos decaying into W or Z bosons [2], and leptoquarks that decay into neutrinos plus jets [3] are examples of new physics models that could contribute events to the jets plus missing E_T topology. In this analysis we look for an event excess in the "monojet" data sample made up of events with a single energetic jet and large $\not\!\!E_T$. Many different models of new physics can produce events with this simple topology. For example, models that involve couplings between SM particles and supersymmetric degrees of freedom which can propagate in a bulk of Extra Dimensions predict increased production of "monojet" events. In fact, if one were to observe a significant excess of signal over the SM prediction in this channel, it would be difficult to identify the exact new physics mechanism responsible for the excess. This difficulty is due to the fact that many of the theories that predict additional signal in this channel are incomplete or involve too many unspecified parameters to be able to determine precise values for their production cross sections. Similarly, in the case where no excess is found, the null result can be generically interpreted for any new physics models that predict event production in our final state. We therefore do not attempt to optimize our analysis for any particular model, but instead concentrate on simple comparisons of the "monojet" data sample with estimates of the SM background contributions in this channel.

Previous searches performed in Run I [4, 5] have not found a significant excess of jets plus missing E_T events over the SM expectation. In this analysis, we are able to significantly improve the sensistivity for observing contributions from new physics processes in the single jet plus $\not\!\!E_T$ event topology by taking advantage of the increase in center of mass energy for Run II $p\bar{p}$ collisions (1.80 TeV to 1.96 TeV), a factor of three increase in the integrated luminosity of our data sample over what was available in Run I, and improved CDF detector performance based on upgrades made prior to the start of Run II. Because of these advantages, we are able to use a robust data-driven approach for the estimate of the SM backgrounds that is less reliant on theoretical calculations than the background estimates made for the Run I analyses. For this analysis we use the larger Run II data samples to directly estimate the electroweak background contributions to our candidate event sample which also has the advantage of reducing systematic uncertainties related to modeling of the background sources such as potential differences between the jet energy scales in data and Monte Carlo.

In the case where no excess is found, we can use our result to set limits on models with compactified Large Extra Dimensions (LED), such as the model of Arkani-Hamed, Dimopoulos, and Dvali (ADD) [6]. The LED scenario is of particular interest since it makes testable predictions about quantum gravity [7] and offers a suitable framework for solving the cosmological constant problem [8]. These models are based on braneworld scenarios where gravity is allowed to propagate in the $4 + n$ dimensional bulk of space-time, while the remainder of the SM fields are confined to the $3 + 1$ dimensional world-volume of the brane configuration. In these LED models, gravitons that are produced directly in processes such as $q\overline{q} \rightarrow gG$, $qg \rightarrow qG$, are $gg \rightarrow gG$ escape undetected in the bulk of extra dimensions, leaving the final state quark or gluon to produce a single jet. In all cases, the resulting event signature is a single jet plus $\not\!\!E_T$. We note that studying these direct production mechanisms offers a more robust test of these LED models than searches for virtual graviton exchange due to the inherent model uncertainties in virtual graviton searches originating from the cutoff scale dependence in the calculation of the expected cross sections.

LED models predict graviton emission in the low energy regime ($\sim$ TeV) because of the relationship between the radius R of the n compactified extra dimensions, the usual Planck mass, and the effective Planck scale M_D as shown in the following expression [6]:

$$M_{Pl}^2 \sim R^n M_D^{2+n}.$$

In fact, if the size of the extra dimensions is large enough ($R \sim \mathcal{O}(10\mu\mathrm{m})$), M_D could potentially be as small as the size of the weak scale (TeV scale), leaving only one fundamental scale for high energy physics. All of the LED model cross section predictions depend on the M_D scale. It is therefore a useful parameter that we can constrain based on our measurement. Note that because the calculation of graviton emission is based on a non-renormalizable, effective low-energy theory that is valid only below the M_D scale and because many other bulk states can contribute to the jets plus missing E_T signal, it is not possible to precisely determine the value of this scale [9]. We can nevertheless determine an absolute lower limit on this fundamental physics scale that is consistent with each of the different LED models. Finally, we note that the direct limits set on M_D via our analysis method have no dependence on non-particle physics assumptions or models in their underlying calculations, as is the case for astrophysical bounds [10]. Thus, even if our resulting limits are less stringent then the astrophysical ones in the cases of $n = 2$ and $n = 3$, they are more robust and could even be used to constrain astrophysical models.

The important components of the CDF II detector used in the reconstruction of the events for this analysis include the tracking system consisting of a silicon-strip vertex detector (SVX II) [11] surrounded by an open-cell drift chamber known as the Central Outer Tracker (COT) [12]. The COT contains eight superlayers of drift cells with twelve sense wires. In order to provide three-dimensional tracking, superlayers of axial wires alternate with $\pm 2^\circ$ stereo angle wires. The tracking system is immersed in a 1.4 T solenoidal magnetic field to allow for the measurement of charged particle momenta transverse to the beamline, p_T. Outside of the magnet, scintillator-based electromagnetic (EM) and hadronic (HAD) calorimeters modules [13] are arranged in projective tower geometries in both the central and forward regions of the detector and used to reconstruct the energy and direction of the particle jets contained within our events. In addition, electromagnetic shower maximum detectors are embedded on the front edge of the EM calorimeter modules. These detectors are used to make higher-precision position measurements for the electromagnetic showers reconstructed within the calorimeter that allow us to better match these showers with electron track candidates. The outermost detection system consists of planes of multi-layered drift chambers for detecting muons [14]. The muon chamber coverage utilized in this analysis corresponds to a pseudorapidity range of $|\eta| < 1.0$ where $\eta \equiv -\ln[\tan(\theta/2)]$ and θ is the angle of a particle with respect to the z-axis. A complete description of the CDF II detector is given in [15].

The data sample used for this analysis was collected with a high E_T single jet trigger. To eliminate non-collision background events such as those originating from beam halo, cosmic rays, and detector noise from our data sample, we require that the highest E_T jet in each event is central ($|\eta| < 1.0$) and does not point at uninstrumented areas of the calorimeter. We also require an event vertex reconstructed from six or more tracks that is within 60 cm of the detector center in z (the detector coordinate parallel to the nominal direction of the colliding beams). Each reconstructed jet with $E_T > 20$ GeV is required to have matching reconstructed tracks whose sum p_T corresponds to at least 10 % of the jet E_T. In the case of the leading E_T jet, we further restrict ourselves to the sum p_T of matching tracks which are also found to point back to a small window around our reconstructed event vertex. Using this tighter track selection criteria, we relax our requirement on the ratio of the track sum p_T over jet E_T from 10 % to 5 % but additionally require that at least two matching tracks contribute to the p_T sum. Finally, to eliminate events from non-beam background particles travelling in the accelerator tunnel that enter the hadronic portion of the calorimeter and produce fake jets, we additionally require that for each event the E_T-weighted electromagnetic energy fraction of all jets with E_T >20 GeV is at least 10 %.

To select the final events for our "monojet" candidate sample, we use a threshold of 150 GeV for the leading jet. Based on this threshold, the single high E_T jet trigger is > 99 % efficient [16] for the events in our sample. To increase the acceptance for events which contain a second jet originating from radiative effects, we accept events that contain a second jet with $E_T < 60$ GeV. However, events that contain three or more reconstructed jets with $E_T > 20$ GeV are removed from the sample. We also require 120 GeV of missing E_T in each event, a selection criteria that is closely coupled to our minimum requirement on the E_T of the leading jet. Cutting slightly lower on $\not\!\!E_T$ allows us to increase the acceptance for possible signal events without suffering a substantial increase in the QCD background. QCD backgrounds which arise from multi-jet events in which one or more of the jets are badly mis-measured in the detector are further reduced by requiring that the direction of the observed $\not\!\!E_T$ does not point within a small cone ($\Delta R < 0.3$) around the direction of the second jet.

The resulting candidate sample contains a significant number of events originating from SM processes that produce events with a similar topology to that of our signal with either real or fake $\not\!\!E_T$. The largest SM background is expected to originate from Z plus jets production where the Z boson subsequently decays into neutrinos ($Z \to \nu\nu$). This process produces events with jets and large, real $\not\!\!E_T$; and since these events basically mimic our signal, the resulting background is irreducible. We expect that the next most significant SM background will come from $W \to \ell\nu$ plus jets production ($\ell = e$, μ, or τ) where the lepton from the decay of the W boson is lost into an uninstrumented region of the detector leading to the production of fake $\not\!\!E_T$ within the event. We attempt to further reduce this particular background by rejecting events from our candidate sample with "lepton-like" objects. In particluar, we reject events which contain any $E_T > 20$ GeV jets with electromagnetic energy fraction greater than 90 % (e candidates) or any isolated, reconstructed track with $p_T > 10$ GeV/c (e, μ, or τ candidates). Track isolation is defined using the measured energy in the calorimeter within a medium-size cone ($\Delta R < 0.4$) around the reconstructed track after subtracting out the measured energy in those towers directly intersected by the track. Tracks are defined to be isolated if this energy is less than 10 % of the measured track p_T. We refer to the collective backgrounds from Z and W boson plus jets production as our electroweak backgrounds. As mentioned above, we also expect to observe some events from QCD multi-jet production where the $\not\!\!E_T$ arises from the mis-measurement of one or more of the jets. We expect that only a small residual background from this source will remain after applying the previously described cuts used to remove these events.

The data-driven strategy used to estimate the number of electroweak background events in our candidate sample is the following. First, we measure the cross sections for $Z \to ee$ plus jets and $Z \to \mu\mu$ plus jets production by selecting events with two identified leptons from independent data samples collected using the high E_T single electron and high p_T single muon triggers. The measured cross sections are for the fraction of Z plus jets events that also satisfy the full set of selection criteria associated with the "monojet" candidate sample after careful removal and/or modification of all measured event quantities to exclude contributions from the reconstructed leptons in these events. For example, the selection cut on missing E_T is applied after the $\not\!\!E_T$ is adjusted to remove the energy associated with the lepton pair produced in the Z boson decay. Using these measured Z plus jets cross sections and the known Z boson branching fractions for leptons and neutrinos, we can obtain two independent estimates for the expected number of $Z \to \nu\overline{\nu}$ plus jets background events in our candidate sample. In addition, we can similarly measure the $W \to e\nu$ plus jets and $W \to \mu\nu$ plus jets cross sections in these data sets and then divide the resulting values by a theoretical prediction for R, the ratio of the W plus jets and Z plus jets production cross sections, to obtain two additional, independent estimates for the expected number of $Z \to \nu\overline{\nu}$ plus jets events in our candidate sample. Finally, we can combine the results of all four measurements to obtain our most precise prediction for the expected background. The advantage of relying only on a theoretical value for R for evaluating the $Z \to \nu\overline{\nu}$ plus jet cross section as opposed to using a purely theoretical estimate is that the theoretical uncertainty on R is significantly smaller than the uncertainties on the individual W plus jet and Z plus jet cross section calculations. This difference is due to the fact that changes in the W plus jets cross section calculation that arise from variations in PDFs or renormalization scale tend to closely follow changes in the Z plus jet cross section calculation for the same variation. Because of these correlations, the associated cross section uncertainties tend to cancel in R. The estimation of other electroweak backgrounds including those from $W \to \ell\nu$ plus jet are also obtained from the measured W/Z plus jets cross sections based on relative acceptance measurements made from simulated event samples.

To select the $W \to \mu\nu$ plus jets and $Z \to \mu\mu$ plus jets events used to make the cross section measurements described above, we make use of two different classes of muon candidates (those with and without matching, reconstructed stubs in the muon detectors). A stubless muon is essentially an isolated track (using the isolation definition described previously) with five or more hits on three or more axial COT superlayers and two or more stereo COT superlayers. The track is also required to have $p_T > 20$ GeV/c, a measured impact parameter in z within 60 cm of the detector center, and a measured impact parameter of less than 0.25 cm (0.025 cm if the track has three or more silicon hits) in $x-y$ with respect to the measured beamline position. We also require that total electromagnetic and hadronic energies measured within calorimeter towers intersected by the track are less than 2 GeV and 6 GeV respectively, consistent with the expectations for a minimum ionizing particle. For tracks with $p_T > 100$ GeV/c, these cut values are gradually increased as a function of the track p_T to maintain high muon selection efficiency. Muon candidates with stubs are required to have either matching stubs in the two most most central CMU and CMP muon detectors ($|\eta| < 0.6$) or a matching stub in the more forward CMX muon detectors ($0.6 < |\eta| < 1.0$). The position of reconstructed stubs is required to be within 3 cm (CMU), 5 cm (CMP), and 6 cm (CMX) of extrapolated track positions along the direction perpendicular to that of the incoming track within the drift plane of the chamber. To ensure that muon candidates with a matching stub are good trigger candidates, we also require that the associated tracks pass through each of the eight COT superlayers.

Similarly, we use two sets of electron criteria to select $W \to e\nu$ plus jets and $Z \to ee$ plus jets events. For this analysis, we only utilize electron candidates in the most central part of the detector ($|\eta| < 1.0$). A loose electron candidate is a track with $p_T > 10$ GeV/c that points at a reconstructed calorimeter energy cluster with $E_T > 20$ GeV. The ratio of hadronic to electromagnetic energy in the cluster must be less than $0.055 + 0.00045 \cdot E$ where E is the total energy of the cluster. As in the case of muon candidates, the track is required to have five or more hits on three or more and two or more stereo COT superlayers in addition to a measured impact parameter in z within 60 cm of the detector center. Loose electron candidates identified as originating from the conversion of a photon into an e^+e^- pair by the standard CDF algorithm are also rejected. For tight electrons the energy cluster in the calorimeter is required to have $E_T > 25$ GeV. In addition, the ratio of the cluster E_T to the track p_T is required to be between 0.5 and 2.0, and the non-electron energy (corrected for leakage) in a medium size cone ($\Delta R < 0.4$) around the electron candidate cluster is required to be less than 10 % of the total cluster energy. We also cut on how well the position of the extrapolated track candidate at the inner edge of the electromagnetic calorimeter modules agrees with the position of the electron cluster candidate as measured by the showermax detector. In the direction parallel to the detector z-axis, the positions are required to match within 3 cm. In the plane perpendicular to the z-axis, we cut on $Q \cdot \Delta x$ where Q is the electron candidate charge ($\pm$ 1) and Δx is the position difference along the axis perpendicular to the incoming track. Using this quantity, we accept electron candidates in the range between -3.0 cm and 1.5 cm. The asymmetric cut is used to maintain a high selection efficiency for electrons that radiate energetic photons. Finally, the lateral shower development observed for the electron candidate is required to be close to that expected for an electron and the calculated χ^2 for the match between the signal observed on the showermax strip cluster and the expectation for a real electron must be less than 10.

We select $W \to \mu\nu$ plus jets events by requiring one muon candidate with a stub using the criteria described above. For this sample only, we also require that the muon candidate track fit based solely on COT hit information has a χ^2 per degree of freedom less than 3.5. This extra requirement helps to reduce muon backgrounds originating from in-flight decays of pions and kaons. In addition, we require that there are no isolated tracks (using the previously described definition) within the event aside from the track associated with the single muon candidate. Finally, we require the event missing E_T is greater than 20 GeV. Before making this cut, the raw $\not\!\!E_T$ observed in the calorimeter is corrected to account for jet energy corrections applied at the analysis level and for the muon which deposits only a small fraction of its energy in the calorimeter. Two muon candidates, one of which satisfies the full set of criteria for a stubbed muon, are required for $Z \to \mu\mu$ plus jets candidate events. The two candidates must have an invariant mass between 66 GeV/c^2 and 116 GeV/c^2 and a three-dimensional opening angle less than 3.07876 radians. For both muon candidate samples, we also run a cosmic track fitting algorithm [17] that uses COT hit-timing information to look for potential cosmic ray track candidates. Using each muon candidate as a seed track for the algorithm, events are rejected if the algorithm is able to reconstruct an extended track passing through two opposite hemispheres of the detector along a common trajectory. For $W \to e\nu$ plus jets candidate events, we require one tight electron and a minimum event missing E_T of 25 GeV. As in the case of muon candidate events, the raw $\not\!\!E_T$ is corrected to account for jet energy corrections applied at the analysis level. However, these jet corrections are not appropriate for electron candidates, and hence no corrections are applied to the raw $\not\!\!E_T$ in conjunction with the one jet associated with the electron. Also, as in the case of muon events, we require that there is no more than one isolated track in each event (based on the previous definition). Finally, $Z \to ee$ plus jets events are required to contain two electron candidates, one of which satisifies the tight selection criteria, with an invariant mass between 66 GeV/c^2 and 116 GeV/c^2.

We measure inclusive cross sections based on these candidate samples and compare the results against published Run II measurements [18] to validate our event selection and techniques for obtaining selection efficiencies and measuring background contributions for the samples. Then, after careful removal and/or modification of all measured event quantities to exclude contributions from the reconstructed leptons in these events, we apply our complete set of "monojet" cuts to the events in these samples. Based on this procedure, selected events are required to have no *extra* isolated tracks, beyond those directly associated with the lepton candidates, as opposed to our stricter requirement of no isolated tracks whatsoever for the events that make it into the missing E_T plus jets candidate sample. Similarly, the missing E_T selection criteria applied to these samples are based on modified values in which energies associated with the reconstructed leptons in the events have been removed (jets matched to reconstructed electron candidates are also removed from the list of jets used in event selection). The cross section measurements used to extract the electroweak background fractions for our final candidate sample are those based on events selected using the default minimum E_T cut of 150 GeV on the leading jet. We also measure cross sections based on events selected with equivalent criteria but utilizing lower thresholds on the leading jet E_T (60 GeV, 90 GeV, and 120 GeV). Because the statistics in the resulting event samples are larger, we are able to make statistically significant comparisons between our independent measurements in the electron and muon samples and obtain further validation of our results. Using standard CDF good run lists, the integrated luminosities of the datasets used to make these cross section measurements are 368 pb^{-1} for electron samples and 356 pb^{-1} for the muon samples.

Acceptances for the W/Z plus jets candidate samples are determined using simulated PYTHIA samples. Standard CDF scale factors are applied to account for measured differences in lepton selection criteria in data versus Monte Carlo. Background calculations are also based on the relevant PYTHIA samples except for QCD backgrounds where we employ the standard technique of studying $\not\!\!E_T$ vs. isolation in both the data and Monte Carlo samples. Using these techniques, we measure the cross sections shown in Fig. 1. We combine the cross section measurements made for the electron and muon samples using the default cut of 150 GeV on the E_T of the leading jet and obtain

$$\sigma(W \to \ell\nu + \text{jets}) \;=\; 0.46 \;\pm\; 0.05 \text{ pb}$$

and

$$\sigma(Z \to \ell\ell + \text{jets}) \;=\; 0.08 \;\pm\; 0.02 \text{ pb}.$$

These cross sections include small correction factors (on the order of 5-10 %) to account for small differences in the event topologies for $Z \to \nu\nu$ and $Z \to \ell\ell$ production. For example, electroweak radiation from charged leptons can produce extra jets within an event that would not be seen in association with neutrinos. Similarly, by removing the jets associated with electrons in the $W \to e\nu$ plus jets and $Z \to ee$ plus jets candidate samples, we exclude some fraction of the available phase space for extra jets within the event (phase space that is available within $Z \to \nu\nu$ events). The correction factors are based on studies of simulated event samples.

Based on these measured cross sections, the cross section for the $Z \to \nu\nu$ plus jets background contribution to the "monojet" candidate sample is obtained using

$$\sigma(Z \to \nu\overline{\nu} + \text{jets}) \;=\; 6 \times \sigma(Z \to \ell\ell + \text{jets})$$

and

$$\sigma(Z \to \nu\overline{\nu} + \text{jets}) \;=\; 6 \times \sigma(W \to \ell\nu + \text{jets}) \times \text{R}$$

where R is the previously described theoretical prediction for the ratio of the W plus jets and Z plus jets production cross sections. To obtain a good result, the theoretical errors on R must be small compared to errors on the measured W plus jet cross sections. Based on discussions with the experts [19], a next-to-leading order calculation based on

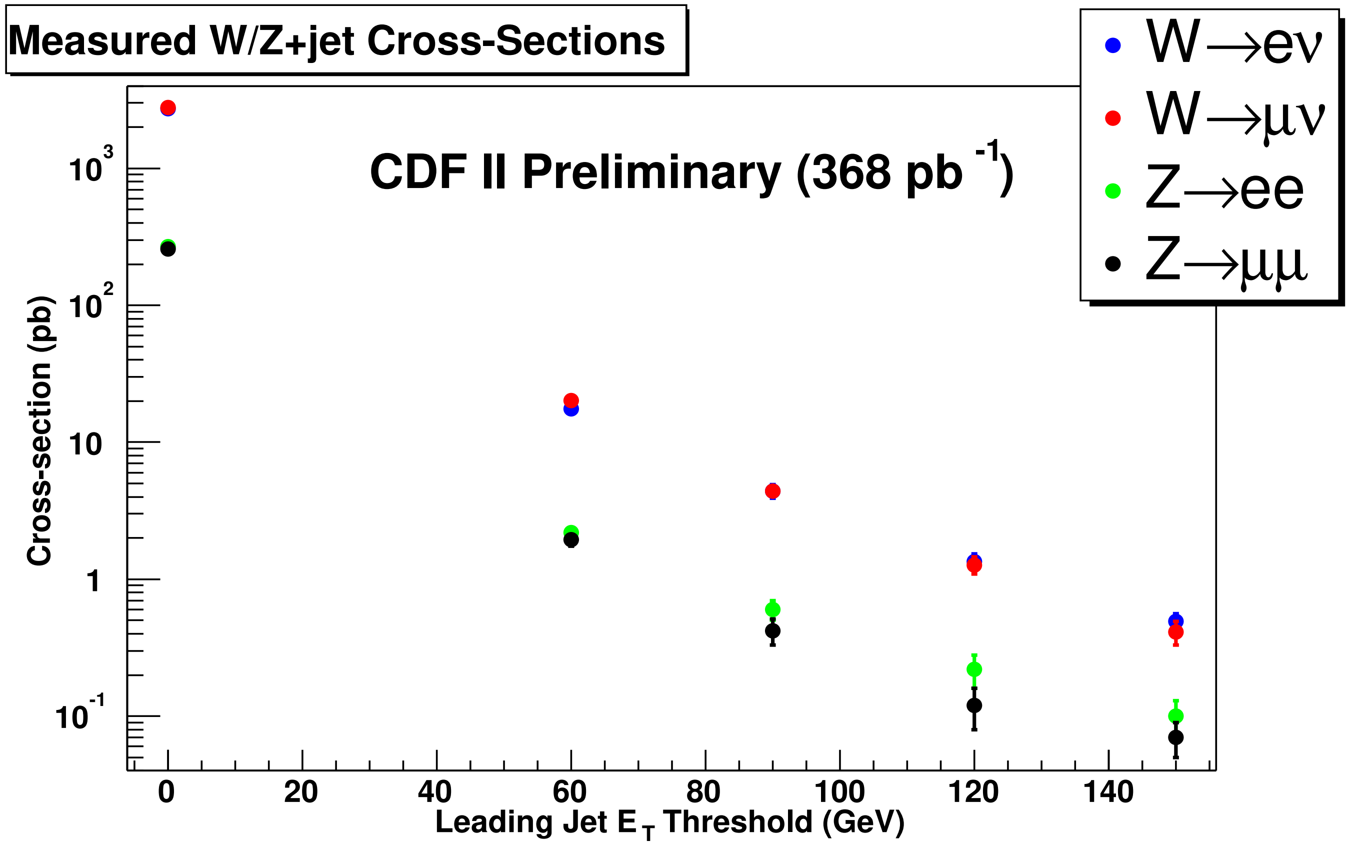

FIG. 1: Cross sections for W and Z+jets as a function of the cut on the leading jet E_T. The results for both muons and electrons are shown. The error bars are statistical only.

the MCFM generator [20] was chosen to determine the value of R. Figure 2 shows the calculated value of R as a function of $P_T^{\rm min}$ for different choices of PDFs and the renormalization and factorization scales. At 150 GeV, the value of R is 8.15 ± 0.40, where the main uncertainties come from PDFs (± 0.09), renormalization scale (± 0.36), and energy scale (± 0.16). The resulting theoretical uncertainty (∼ 5%) turns out to be well below the current level of uncertainties (mostly statistical) associated with our cross section measurements. Using the above expressions we obtain estimates for the number of $Z \to \nu\overline{\nu}$ plus jets events in the 368 pb^{-1} "monojet" candidate sample of 177 ± 44 and 125 ± 15 using the measured $Z \to \ell\ell$ plus jets and $W \to \ell\nu$ plus jets cross sections. The two independent results are combined to obtain our best estimate of the $Z \to \nu\overline{\nu}$ plus jets background in the "monojet" candidate sample (130 ± 14 events). The contributions of the other electroweak backgrounds to the candidate sample are also determined from these measured cross sections based on relative acceptances obtained from simulated event samples.

As described previously, QCD multi-jet events can also enter our sample when one or more jets in the event are badly mis-measured or lost into a detector crack. We identify three main multi-jet event topologies that can contribute events to our candidate sample: (1) dijet events where the second jet is completely lost, (2) three-jet events where two jets are well-measured and the third is lost, and (3) three-jet events where one or both visible jets are mis-measured and the third jet is lost. We determine the relative contributions of the three multi-jet processes using Monte Carlo and use data to measure the absolute contribution of the dijet configuration which is expected to dominate. This estimate is obtained using a sample of dijet events that satisfy the basic selection criteria of our "monojet" candidate sample (leading jet E_T > 150 GeV and event missing E_T > 120 GeV) but for which the event missing E_T points in the same direction as that of the less energetic jet. Note that this last requirement is orthogonal to that used for selecting the events in our final candidate sample (in that case we specifically require that the missing E_T does not point in the direction of the less energetic jet). The E_T distribution for the less energetic jets in this dijet event sample is shown in Fig. 3. In cases where one jet loses so much energy that its E_T drops below the threshold (20 GeV) for defining jets in our analysis, the event topology of our "monojet" candidate sample is reproduced. The magnitude of this background is obtained by making a linear extrapolation of the distribution shown in Fig. 3 into the region below 20 GeV. Based on this extrapolation, we obtain an estimated background of 13 events in the low E_T region

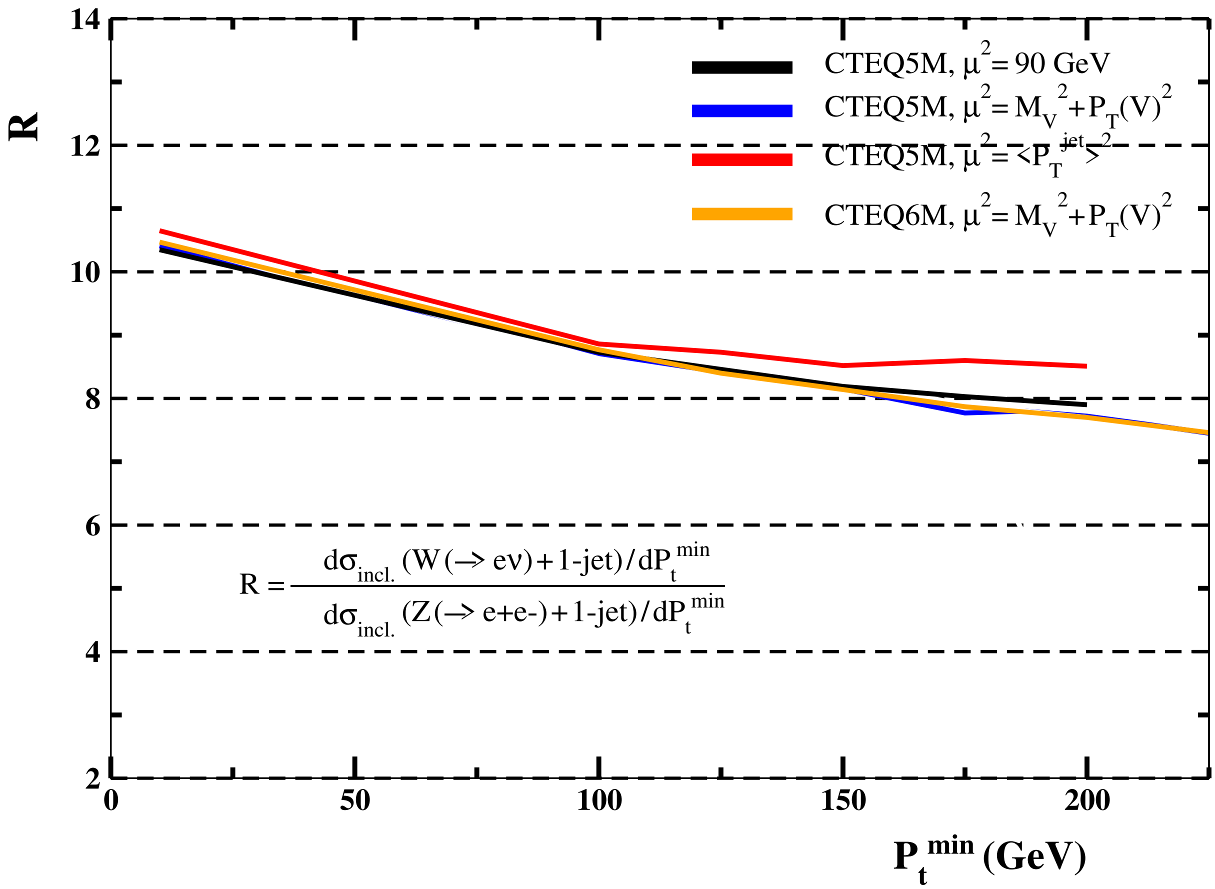

FIG. 2: R as a function of P_T^{min} for several choices of PDFs and renormalization scales.

below the jet threshold. From studies of QCD multi-jet Monte Carlo samples, we determine that the three-jet event topologies described above contribute roughly an additional 15% with respect to the measured dijet contribution. To obtain further confidence in this result, we compare distributions of the difference in ϕ between the missing E_T and less energetic jet for dijet events in the data and Monte Carlo samples (shown in Fig. 4) and observe good agreement. Using this result we estimate that the total QCD multi-jet background contribution to our final candidate sample is 15 ± 10 events where the uncertainty is obtained by varying the extrapolation within its fit uncertainties.

We expect that a few events from non-collision sources such as cosmic rays and beam-related backgrounds will make it into our final candidate sample. A small fraction of these events, especially those that overlap with real collisions, have a non-negligible probability for surviving the cleanup cuts used in this analysis. We use timing information available from the hadronic calorimeter to estimate this small, residual background. We look for events with hadronic energy deposits that are measured to arrive more than 40 ns out-of-time with respect to the nearest collision but less than 80 ns out-of-time with respect to the same collision. The upper limit on the out-of-time requirement is made to avoid energy deposits associated with neighboring collisions. We compare the fraction of events with out-of-time deposits in our final candidate sample and our W/Z plus jet event samples which are expected to contain negligible contributions from non-collision backgrounds. We observe a slightly higher fraction of events of this type in the final candidate sample that is consistent with a non-collision background of 4 ± 4 events. We assign a 100% uncertainty on this estimate to account for the fact that none of these events can clearly be identified as a non-collision event based on event displays. A summary of our background estimates for the various Standard Model processes contributing to the "monojet" candidate sample is shown in Table I. We predict a total SM background of 265 ± 30 and observe 263 events in the data; and therefore conclude that no excess is present in the data. Figure 5 shows a comparison of the missing E_T distribution for the 263 events in our candidate sample with the expected distribution from the SM backgrounds.

Based on these results, we set lower limits on the n-dimensional Planck scale as explained previously. In order to determine these limits, we first evaluate the signal acceptance for graviton events using simulated event samples. The fraction of events in our signal Monte Carlo events that survive our final selection requirements determine the

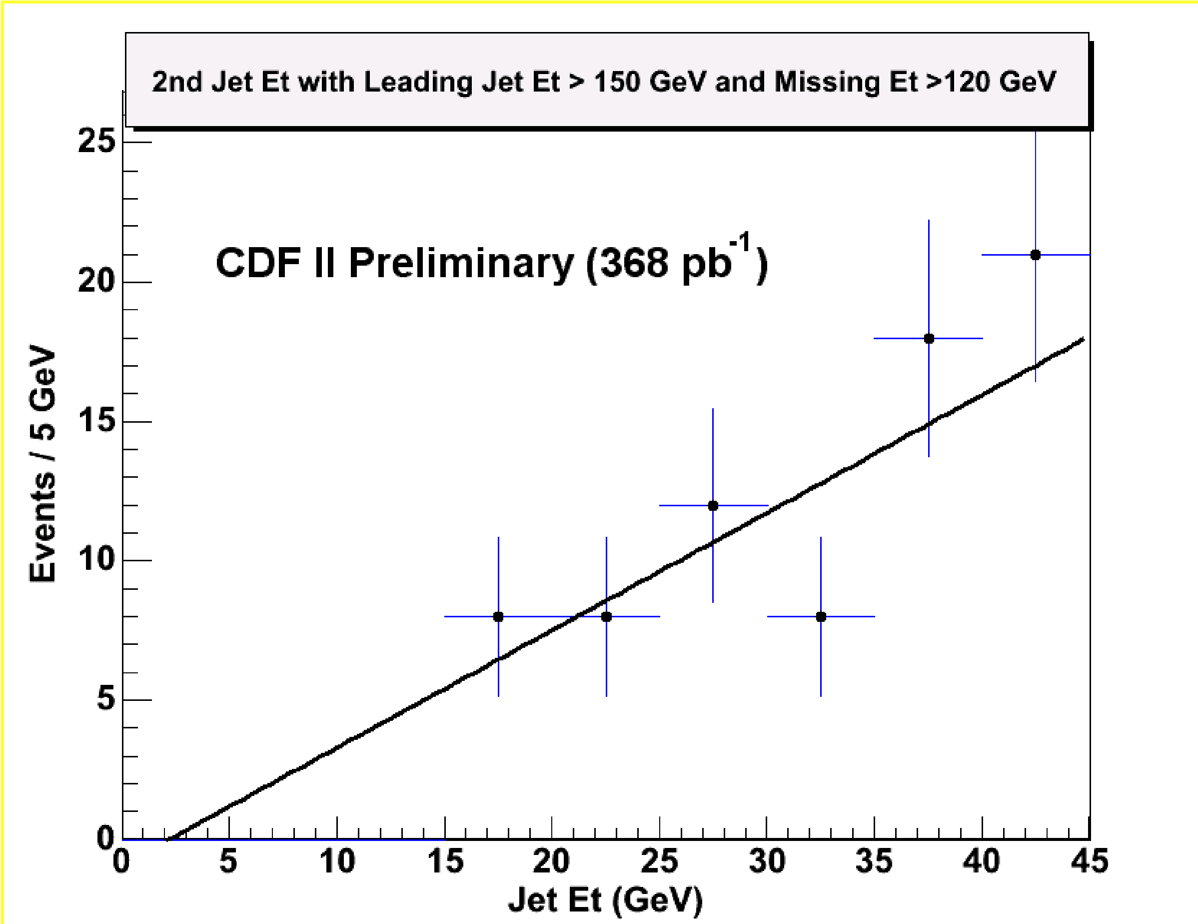

FIG. 3: E_T of the second jet in dijet events, with the extrapolation for the lost jets superimposed.

Background	
$Z \to \nu\overline{\nu}$	130 $\pm$ 14
$W \to \tau\nu$	60 $\pm$ 7
$W \to \mu\nu$	36 $\pm$ 4
$W \to e\nu$	17 $\pm$ 2
$Z \to \ell\ell$	3 $\pm$ 1
QCD	15 $\pm$ 10
Non-collision	4 $\pm$ 4
Total predicted	265 $\pm$ 30
Data observed	263

TABLE I: Summary of the Standard Model background contributions and number of events observed for the "monojet" candidate sample.

acceptances as functions of n and M_D (used as inputs to the signal simulation). In order to compare our results with published DØ results, the generated cross sections are scaled by a K-factor (the expected ratio of cross sections at next-to leading order (NLO) and leading order (LO)) of 1.3 [21]. The cumulative signal acceptance for our selection criteria ranges from 9.9 % to 12.6 % as a function of n and is flat as a function of M_D. Major sources of systematic uncertainty on the acceptance come from the choice of parton structure functions, potential differences in the jet energy scale between data and simulation, and the models for initial and final state radiation (ISR/FSR) in the Monte Carlo. As detailed in [22], our combined estimate for the relative uncertainty on the measured signal acceptances is 13.2 %.

Based on the observed number of events, our estimate of the SM background, and the measured signal acceptances (in conjunction with their associated uncertainties), we set limits on the number of potential signal events in our

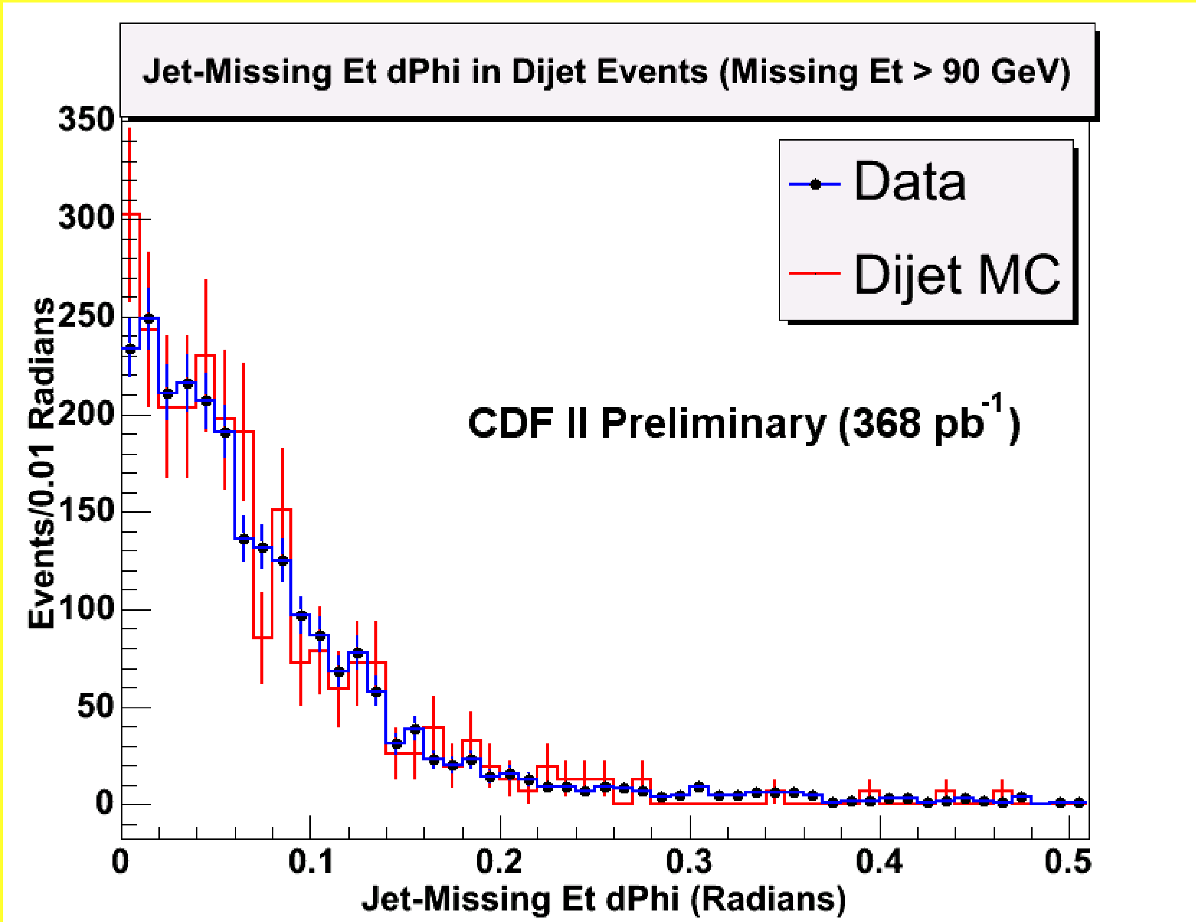

FIG. 4: Comparison of $\Delta\phi(\text{Jet} - \not\!\!E_T)$ in data and MC. To increase the statistics used in the comparison, the cut on $\not\!\!E_T$ has been lowered to 90 GeV.

n	$M_D(K = 1.0)$	$M_D(K = 1.3)$	Run I$(K = 1.0)$	Run I$(K = 1.3)$	LEP Avg
2	1.09	1.16	1.00	1.06	1.60
3	0.93	0.98	–	–	1.20
4	0.87	0.90	0.77	0.80	0.94
5	0.82	0.85	–	–	0.77
6	0.80	0.83	0.71	0.73	0.66

TABLE II: 95 % C.L. limits on M_D in TeV for n = 2-6 compared with limits from Run I measurements and combined LEP averages.

candidate sample. For 263 observed events, a SM expectation of 265 ± 30 events, and a 13.2 % uncertainty on the signal acceptance, we obtain a maximum limit of 70.3 signal events at the 95 % C.L. Next, we set limits on the value of M_D for different values of n based on the maximum possible number of observed signal events. These limits on on M_D for n = 2-6 are shown in Table II for both $K = 1.0$ and $K = 1.3$. A comparison of the limits on M_D from DØ and CDF with the LEP averages is shown in Fig. 6. For $n = 5$ and $n = 6$, our measurement places the world's best limits on M_D. Assuming compactification on a torus, these limits on M_D can easily be related to limits on the radius of the extra-dimension via the expression [7]

$$R^n = \frac{1}{8\pi}\left(\frac{M_{PL}}{M_D}\right)^2 \frac{1}{M_D^n}.$$

For example, in the case of two extra dimensions, we obtain an upper limit of 0.36 mm on the size of the extra dimensions based on the lower limit for M_D (1.16 TeV). To summarize, we perform a search for direct graviton

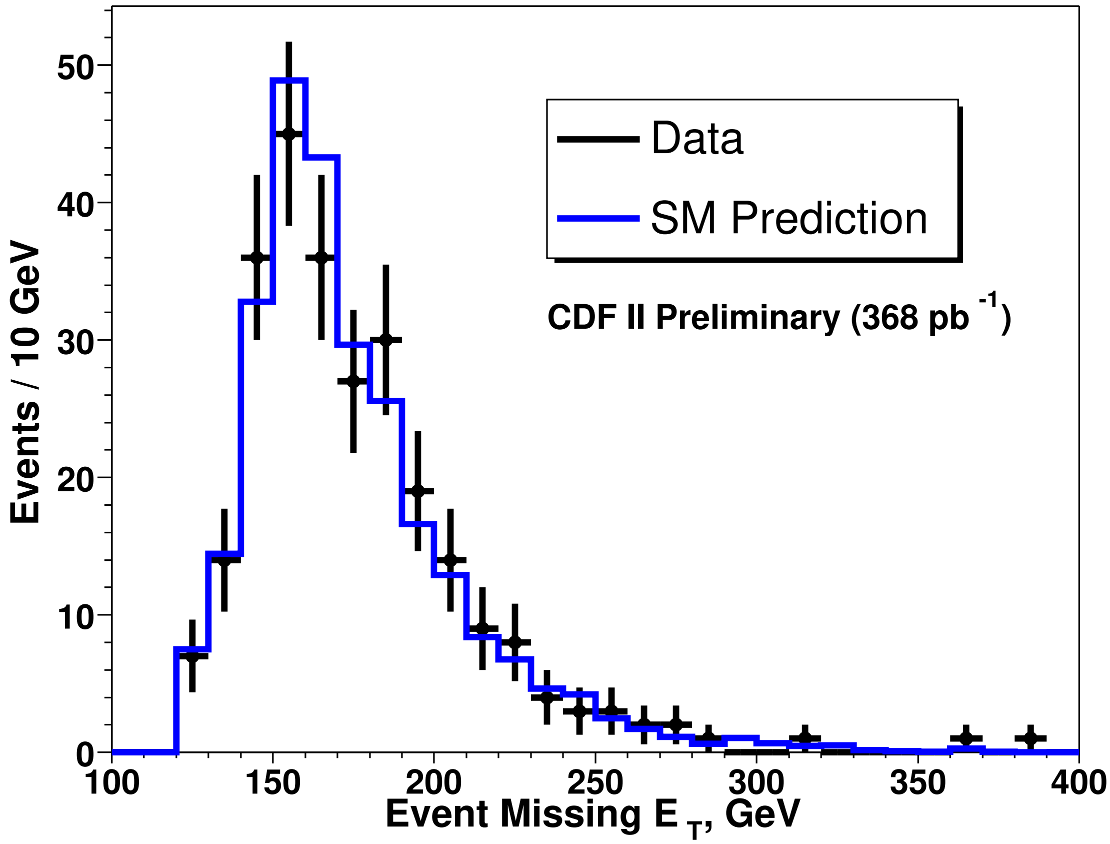

FIG. 5: Comparison of the event missing E_T distribution for the the 263 events in our candidate sample with the predicted SM distribution.

production in a sample of events containing one high E_T jet and large missing E_T obtained from 368 pb^{-1} of CDF Run II data. We find good agreement between the SM background prediction and the observed number of events in our sample and based on this result set lower limits at the 95 % C.L. for the effective Planck scales for n = 2-6 extra dimensions.

We thank the Fermilab staff and the technical staff at the participating institutions for their essential contributions to this research. This work is supported by the U. S. Department of Energy and the National Science Foundation; the Italian Istituto Nazionale di Fisica Nucleare; the Natural Sciences and Engineering Research Council of Canada; the Ministry of Education, Culture, Sports, Science and Technology of Japan; the National Science Council of the Republic of China; the Swiss National Science Foundation; the A. P. Sloan Foundation; the Bundesministerium fuer Bildung und Forschung, Germany; the Korea Science and Engineering Foundation (KoSEF); the Korea Research Foundation; and the Comision Interministerial de Ciencia y Tecnologia, Spain.

---

[1] J.F. Gunion and S. Mrenna, *A Study of SUSY signatures at the Tevatron in models with near mass degeneracy of the lightest chargino and neutralino*, Phys. Rev. D62, 015002 (2000) [hep-ph/9906270]

[2] T. Handa, The CDF Collaboration, *Technicolor Limits at the Tevatron*, CDF note 4936

[3] J.L. Hewett and T.G. Rizzo, *Much ado about leptoquarks: A Comprehensive analysis*, Phys. Rev. D56, 5709 (1998);; S. Hagopian, *Leptoquark summary form the Tevatron*, A CDF and D∅ Collaborations public note.

[4] D. Acosta et al., The CDF Collaboration, *Search for Kaluza-Klein Graviton Emission in $p\bar{p}$ Collisions at $\sqrt{s} = 1.8$ TeV using the Missing Energy Signature*, Phys.Rev.Lett. **92** (2004) 121802.

[5] V.M. Abazov et al., The D0 Collaboration, *Search for large extra dimensions in the monojet + $\not\!\!E_T$ channel with the DZero detector* Phys. Rev. Lett. 90, 251802 (2003).

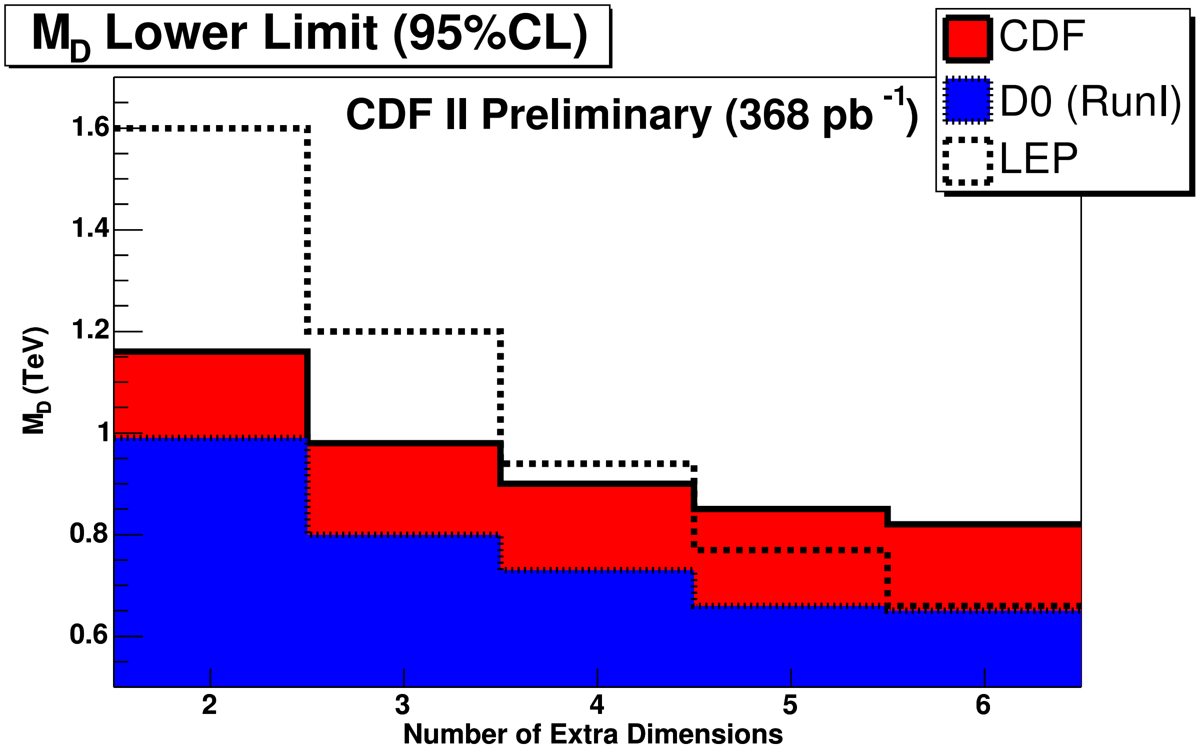

FIG. 6: Comparison of limits on M_D based on the Run II CDF and Run I D∅ results with the combined LEP averages.

[6] N. Arkani-Hamed, S. Dimopoulos, and G. Dvali, *Phys. Lett.* B429 1998; preprint hep-ph/9807344.

[7] G.F. Giudice, R. Rattazzi, J.D. Wells, preprint hep-ph/9811291 v2.

[8] C.P. Burgess, *Toward a natural theory of dark energy: supersymmetric large extra dimensions*, AIP Conf. Proc. **743**, 417-449 (2005) [hep-th/0411140]; C.P. Burgess, *Supersymmetric Large Extra Dimensions and the Cosmological Constant: An Update*, Annals of Physics (to appear) [hep-th/0402200].

[9] G. Azuelos, P.-H. Beauchemin and C.P. Burgess, *Phenomenological Constraints on Extra-Dimensional Scalars*, J. Phys. G: Nucl. Part. **31** 1-19 (2005) [hep-ph/0401125]; D. Atwood, C.P. Burgess, E. Filotas, F. Leblond, D. London and I. Maksymyk, Physical Review D63 025007 (2001) [hep-ph/0007178];

[10] S. Hannestad and G. Raffelt, Phys. Rev. Lett. **87** (2001) 051301, [hep-ph/0103201]; Phys. Rev. Lett. **88** (2002) 071301, [hep-ph/0110067]; Phys. Rev. **D67** (2003) 125008, Erratum-ibid. **D69** (2004) 029901, [hep-ph/0304029]; S. Hannestad, Phys. Rev. **D64** (2001) 023515, [hep-ph/0102290].

[11] A. Sill *et al.*, Nucl. Instrum. Meth. A **447**, 1 (2000)

[12] T. Affolder *et al.*, Nucl. Instrum. Meth. A **526**, 249 (2004)

[13] L. Balka *et al.*, Nucl. Instrum. Meth. A **267**, 272 (1988)

[14] G. Ascoli *et al.*, Nucl. Instrum. Meth. A **268**, 33 (1988);
T. Dorigo, Nucl. Instrum. Meth. A **461**, 560 (2001)

[15] D. Acosta *et al.*, Phys. Rev. D71, 032001, (2005)

[16] F. Chlebana, G. Flanagan, A. Bhatti, J Dittmann, J. Huston, G. Latino, M. Martinez-Perez, R. Snihur, *First Measurement of the Inclusive Jet Cross Section in Run II*, CDF Note 6298.

[17] H. Gerberich, A. Kotwal, C. Hays, *Cosmic Ray Tagging using COT Hit Timing*, CDF Note 6089.

[18] D. Acosta et al., The CDF Collaboration, *First Measurements of Inclusive W and Z Cross Sections from Run II of the Tevatron Collider* Phys. Rev. Lett. 94, 091803 (2005).

[19] Private communication with Steven Mrenna.

[20] Monte Carlo for FeMtobarn processes at Hadron Colliders. J. Campbell and K. Ellis. See `http://mcfm.fnal.gov/`.

[21] Prakash Mathews, V. Ravindran, K. Sridhar, W.L. van Neerven *Next-to-Leading Order QCD Corrections to the Drell-Yan Cross Section in Models of TeV-Scale Gravity*, preprint hep-ph/0411018; Prakash Mathews, V. Ravindran, K. Sridhar, *NLO-QCD Corrections to Dilepton Production in the Randall-Sundrum Model*, preprint hep-ph/0506158.

[22] P.H. Beauchemin, K. Burkett, E. James, P. Savard and A. Yagil, *Search for Extra Dimensions in Jets+Missing Energy in RunII*, CDF Note 7675